Journal of Geophysical Union - Research C - Oceans
July 2003; 108(C7) : NIL_48-NIL_61
http://dx.doi.org/10.1029/2002JC001428

An edited version of this paper was published by AGU.

Impact of rain cell on scatterometer data: 1. Theory and modeling

J. Tournadre and Y. Quilfen

Ifremer, BP 70, 29280 Plouzane, France

*: Corresponding author : Tél.: (33) 298 22 44 97, e-mail: jean.tournadre@ifremer.fr

Abstract:

The two scatterometers currently in operation, the Ku-band NASA Seawinds on the QuikScat satellite and the C-band AMI-Wind on the ERS-2 satellite, are designed to infer the ocean wind vectors from sea surface radar backscatter measurements. They provide excellent coverage of the ocean, and their wind products are of great value for ocean and meteorological communities. However, the presence of rain within scatterometer cells can significantly modify the sea surface backscatter coefficient and hence alter the wind vector retrieval. These perturbations can hamper the analysis of wind fields within atmospheric low-pressure systems or tropical cyclones. Rain perturbations result from volume scattering and attenuation by raindrops in the atmosphere as well as changes of sea surface roughness by impinging drops. For scatterometers operating at Ku-Band, attenuation and volume scattering are strong and one order of magnitude larger than at C-band. The wind retrieval will thus be less affected for the C-band AMI-Wind instrument than for the Ku-band Seawinds. A theoretical model, based on radiative transfer formulation including rain attenuation and scattering, has been developed to quantify the modification by rain of the measured backscatter and of the retrieved wind vectors. Changes in surface roughness, a complex phenomenon not yet fully understood and parameterized, is not considered here although it could be of importance for high rain rates. As a scatterometer cell covers several hundred square kilometers, inhomogeneities of rain within the cell will further modify the measured backscatter, particularly in case of small, intense precipitating rain cells. Using analytical rain cell models and constant wind fields, the effects of partial beam filling by rain is investigated. The model results show that Ku-band scatterometer data are greatly affected by rain and are extremely sensitive to the distribution of rain within scatterometer cells, i.e., to the distance between the rain cell center and the scatterometer resolution cell center. When the scatter from the sea surface is low, the additional volume scattering from rain will have a marked effect leading to an overestimation of the low wind speed actually present. Conversely, when the backscatter is already high (at high winds), attenuation by rain will reduce the signal causing an underestimation of the wind speed. The wind direction is modified in a complex manner and mainly depends on the rain distribution within the scatterometer cell. These results show that, especially at low and moderate wind speed, rain data such as the Special Sensor Microwave/Imager (SSM/I) rain fields are too coarse for correction of Normalized Radar Cross Section (NRCS) and that high-resolution rain data (such as the Tropical Rainfall Mapping Mission (TRMM) ones) are necessary. They also show that a good rain flagging is still an important issue for the operational use of Ku-band scatterometer data. A succeeding paper will present an example of application of the model for the correction of QuikScat data using TRMM rain data within a tropical cyclone.

1 - Introduction

The two scatterometers currently in operation, Seawinds on QuikScat and AMI-wind on ERS-2, were designed to measure speed and direction of the global ocean surface wind. They both employ radar, in Ku-band (13.4 GHz) for Seawinds and C-band (5.6 GHz) for AMI-WIND, to measure the sea surface backscatter at multiple azimuths, incidences and polarizations from which wind speed and direction are inferred using semi-empirical models. These two sensors provide an excellent coverage of the ocean and their wind products are of great value for ocean and meteorological communities (a short description of AMI-WIND and Seawinds scatterometers is given in Appendix A). However, experiences with the Seasat, NSCAT and ERS-1 scatterometers have indicated that the presence of rain can severely alter wind measurements *[Guymer et al, 1981][Moore et al., 1983][Smith and Wentz, 1998][Quilfen et al., 1998]*. During the calibration/validation phase of Seawinds, this contamination of the wind retrieval by rain quickly became apparent, especially in tropical regions. Since there is no sensor on QuikScat to measure rain coincidentally with the scatterometer measurement, the current approach has been to flag the data that may be contaminated. Two rain detection algorithms have been defined based on an empirically normalized objective function *[Mears et al., 1999]* and multidimensional histograms *[Huddleston and Stiles, 2000]*. They are used to define a rain flag in the level2B Seawinds products, and they are still considered of research quality.

Few studies, *[Moore et al, 1982][Moore et al., 1983][Yueh et al., 2001],* have investigated the effects of rain on Ku-band scatterometer measurements. They were limited to simple radiative transfer models and assumed scatterometer cells filled with homogeneous rain layers. However, past experiences with TOPEX/Poseidon Ku-band altimeter data showed that partial beam filling and rain inhomogeneities within the measurement cell can further alter the retrieval of geophysical parameters *[Quartly, 1998][Tournadre, 1998]*, especially in case of small intense rain cells which are difficult to detect using passive microwave data. In this paper, we present a model of interaction between rain cells and scatterometer radar signal. This model is used to compute the Normalized Radar Cross Section (NRCS) measured by a scatterometer in presence of a rain cell. From these NRCS modeling results, the errors induced by rain on the quality of the wind retrieval can also be estimated. In this Part I paper, the model is extensively used to quantify the signature of analytical rain cells on Seawinds NRCS and retrieved wind vectors. A succeeding paper will present an example of application of the model to real QuikScat and Tropical Rain Mapping Mission data for a tropical cyclone.

The model of computation of the rain modified surface NRCS is described in section 2 as well as the analytical rain cell model used in this study. Section 3 presents the modeling results for Seawinds. Section 3.1.1 investigates the NRCS modification assuming a constant surface NRCS within a rain cell and sections 3.1.2 and 3.1.3 generalize the results to a large range of rain cell characteristics. The influence of rain cells on the quality of the wind retrieval is studied in section 3.2. Section 4 briefly describes the model results obtained for the C-band AMI-Wind scatterometer configuration. The conclusions and the perspectives are presented in section 5.

2 - Radar signature of rain cells: Model of rain interaction

Rain drops within the atmosphere have three possible effects on microwave signals. Firstly, rain drops scatter some energy of the incident signal back to the sensor, and thus increase the power backscattered to the scatterometer. Secondly, rain drops absorb the signal causing an extinction of the signal. Thirdly, the rain drops striking the ocean surface alter the surface roughness and hence the radar cross section. Experiments performed in wind-wave tanks have shown that the surface roughness change by rain drops could be a significant error source in wind retrieval from scatterometer data [Bliven and Giovanangeli, 1993][Sobieski et al., 1999] [Craeye and Schlüssel, 1998]. However, the existing experimental data set at Ku and C-band which are the principal scatterometer operating bands, does not easily lend itself to scatterometer performance modeling due to the limited range of incidence angles, wind azimuth angles and polarizations examined. For these reasons, our model will only address the atmospheric effects of rain. However, if a parametrization of the modification of the surface radar cross section by rain becomes available, it could be easily included into the model.

The attenuation and volume scattering effects of rain drops have been widely studied since the 1940's and the literature on the subject is plentiful. Several formulations based on the Mie scattering theory are available in the literature *[Marshall and Palmer, 1948][Ulaby et al., 1981]* and will be used in this study.

2.1 - Radiative transfer model

Following *[Ulaby et al., 1981]*, the radiative transfer equation for microwaves through an homogeneous layer of rain can be written as follows using the coordinate system presented in figure 1:

$$dI_+(z) = -k_a I_+(z)\,dz\,sec(\theta)$$
$$dI_-(z) = -\eta I_+(z)\,dz\,sec(\theta) + k_a I_-(z)\,dz\,sec(\theta) \quad (1)$$

where I_+ and I_- are the down and upwelling power; η is the volume backscatter coefficient, k_a is the attenuation coefficient (dB.km^{-1}) and θ the incidence angle.

These differential equations are of first order and have standard solutions of the form:

$$I_+(z) = I_+(0)e^{-k_a z sec(\theta)}$$
$$I_-(z) = I_-(d)e^{k_a(z-d)sec(\theta)} + \int_d^z \eta I_+(0)e^{2k_a z' sec(\theta)} sec(\theta)\,dz' \quad (2)$$

where *d* is the lower boundary (sea surface) abscissa.

If σ_0 is the surface backscatter coefficient of the lower boundary, and if *H* is the height of the rain layer then the boundary conditions can be expressed as follows

$$I_+(d) = I_+(0)\,e^{-k_a H sec(\theta)}$$
$$I_-(d) = \sigma_0 I_+(d) = \sigma_0 I_+(0)\,e^{-k_a H sec(\theta)} \quad (3)$$

where $I_+(0)$ is the power of the emitted pulse.

By simple integration the power received by the antenna, $I_-(0)$, can be expressed as

$$I_-(0) = I_+(0)\sigma_0 e^{-2k_a H sec(\theta)} + \eta I_+(0)\frac{1}{2k_a}(1 - e^{-2k_a H sec(\theta)}) \quad (4)$$

Thus, the rain modified NRCS , $\widetilde{\sigma_0}$, measured by the sensor is

$$\widetilde{\sigma_0} = \frac{I_-(0)}{I_+(0)} = \sigma_0 e^{-2k_a H sec(\theta)} + \eta \frac{1}{2k_a}(1 - e^{-2k_a H sec(\theta)}) \quad (5)$$

The first term of the right hand size of equation (5) represents the attenuation term and the second one the volume scattering. The attenuation coefficient by rain, k_a, is related to the rain rate, *R*, by the Marshall-Palmer relation *[Marshall and Palmer, 1948]*,

$$k_a = a\,R^b \quad (6)$$

where *a* and *b* are frequency dependent coefficients. At Ku-band (13.4 GHz), the *a* and *b* coefficients are

respectively 0.0314 and 1.14 *[Slack et al, 1994]* (at C-band, a=1.06 10^{-3} and b=1.393 *[Olsen et al, 1978]*). Clouds, water vapor and ice particles can also contribute to attenuation, but in general these additional contributions are comparatively small and can be considered as negligible *[Spencer and Shimada, 1991][Ulaby et al., 1981]* in this analysis. The volume scattering coefficient, η (in m^{-1}), depends on reflectivity, Z (in mm^6m^{-3}), and rain rate, R, by *[Ulaby et al., 1981]*

$$\eta = \frac{\pi^5}{\lambda_0^4} 10^{-18} |K_0|^2 Z \quad (7)$$

and *[Doviak and Zrnic, 1984]*

$$Z = 400 R^{1.4} \quad (8)$$

where, λ_0, denotes the radar wavelength and K_0 is a quantity which describes the scattering efficiency of the hydrometeors.

Figure 2 illustrates the model $\widetilde{\sigma_0}$ for a Ku-band radar as a function of rain rate for a surface NRCS varying from -35dB to 5dB at 46° incidence. This represents the effect of homogeneous rain filling completely a scatterometer resolution cell. For low NRCS (corresponding to low wind speed) the scattering by rain is dominant and can largely exceed 10 dB for rain rates greater than 10 mm/hr. This will lead to an overestimation of wind speed. For higher NRCS and winds, attenuation is dominant until 15mm/hr leading to an underestimation of wind speed. For rain rates exceeding 20 mm/hr, the contribution from surface backscatter to $\widetilde{\sigma_0}$ is much smaller than scattering by rain. $\widetilde{\sigma_0}$ thus becomes almost independent of the surface NRCS and converges to an almost constant value of -11dB. For high rain rates, the retrieval of a surface wind vectors becomes almost impossible without a precise knowledge of the rain rate.

2.2 - Effective normalized radar cross section within a rain cell

The rain modified NRCS estimated using equation (5) only represents the case where a scatterometer resolution cell is completely filled by homogeneous rain. That is rarely true in nature. In general, the horizontal rain structure within a weather system is smaller than the dimension of a scatterometer resolution cell. This, coupled to the non linearity of the effect of precipitation, implies that the assumption of homogeneous rain layer may not yield realistic results.

Within a rain cell over the ocean, the radar signature is composed, as shown by equation (5), of contributions from volume scattering and attenuation by rain drops in the atmosphere as well as from surface scattering by sea surface roughness. The backscatter from all hydrometeors that have the same range to the sensor are mapped onto the same radar range bin *[Melsheimer et al, 1998]*. This contribution from volume backscatter, which is also affected by attenuation due to the presence of rain in the atmosphere, is added to the contribution from backscatter at the sea surface. Using equation (5) the effective NRCS for a point *M(x,y)* is given by *[Melsheimer et al, 1998]*

$$\widetilde{\sigma}_0(x,y)=\sigma_0(x,y)\exp\left(-2\int_0^{f(y)}k_a(u)\,du\right)+\sin\theta\int_0^{l(y)}\eta(s)\exp\left(-2\int_0^{f_y(s)}k_a(u)\,du\right)ds \quad (9)$$

where y is the ground range coordinate, $l(y)$ is the length of the rain filled tilted column contributing to the effective NRCS, $f_y(s)$ is the boundary of the rain cell as a function of the coordinate s of the tilted column with the origin at y, and $f(y)$ is the path length of radar signal at range y.

The main problem to compute $\widetilde{\sigma}_0$ is thus to estimate f, l, f_y, k and η for a given rain cell. If the rain rate were known at every space point (x,y,z), equation (9) could be numerically integrated. However, this would be very computer time consuming and this can not be done to estimate the effect of rain for a large range of rain cells. Under some simplifying hypothesis the influence of rain cells can be more easily studied and analyzed.

2.3 - Computation of the path and tilted column length

Assuming a cylindrical rain cell of diameter d and height h, it can be easily shown by using simple geometrical consideration (see figure 3-b), that the path length, f and the tilted column length, l, have the following form

$$f(y)=min\left(max\left(0,\frac{y-y_1}{\sin\theta}\right),\frac{h}{\cos\theta}\right)-min\left(max\left(0,\frac{y-y_2}{\sin\theta}\right),\frac{h}{\cos\theta}\right) \quad (10)$$

$$l(y)=min\left(max\left(0,\frac{y_2-y}{\cos\theta}\right),\frac{h}{\sin\theta}\right)-min\left(max\left(0,\frac{y_1-y}{\cos\theta}\right),\frac{h}{\sin\theta}\right)$$

where y_1 and y_2 are the near and far range coordinates of the rain cell edges (figure 3). The upper boundary of

the cell $f_y(s)$, in the tilted local coordinate system (*M*,*s*,*u*) can be computed using the same geometrical considerations by

$$\begin{aligned} \mathrm{le}_y(s) &= -\tan\theta\, s + \frac{h}{\cos\theta} \\ f_1(s) &= min\left(max\left(0, \frac{(s - s_1)}{\tan\theta}\right), \mathrm{le}_y(s)\right) \\ f_2(s) &= min\left(max\left(0, \frac{(s - s_2)}{\tan\theta}\right), \mathrm{le}_y(s)\right) \\ f_y(s) &= f_1(s) - f_2(s) \end{aligned} \quad (11)$$

where le_y, f_1 and f_2 represent the equations of the rain cell boundaries in the local coordinate system and $s = (y - y_0)/\cos\theta$. It should be noted that $f(y) = f_y(0)$.

Rain rate is assumed constant along the tilted path lengths (i.e. along lines of constant *s*). This introduces a small computational error, but allows a great simplification of $\widetilde{\sigma}_0$ computation. Indeed, using (10) and (11), equation (9) becomes

$$\widetilde{\sigma}_0(x,y) = \sigma_0(x,y) e^{-2k_a(x,y)f(y)} + \frac{\sin\theta}{2} \int_0^{l(y)} \eta(s) \frac{1}{k_a(s)} e^{-2f_y(s)k_a(s)} ds \quad (12)$$

Knowing the rain rate field, $R(x,y)$, within the rain cell, equation (12) can easily be numerically integrated using

$$\begin{aligned} k_a(x,y) &= 2aR^b(x,y) \\ \eta(s) &= \frac{\pi^5}{\lambda_0^4} 10^{-18} |K_0|^2 400 R(x + s\cos\theta, y + s\sin\theta)^{1.4} \end{aligned} \quad (13)$$

2.4 - Rain cell model.

Past studies of the effect of rain on TOPEX/Poseidon waveforms *[Tournadre, 1998][Quartly, 1998]* have shown that it is easier to test and to quantify the influence of rain cells on satellite measurements using analytical rain cell models than measured rain fields. Several studies based on the analysis of meteorological radar data have been published on the size of rain cells and on the distribution of rain rate within the cell. Among them *[Goldhirsh and Musiani, 1986] [Capsoni et al., 1987]* have been used in this study. These studies showed that, the rain rate fall-off within a cell can be represented by exponential or Gaussian fall-off.

For simplicity, we used a cylindrical Gaussian rain cell model of radius *r* and constant height, *h*, defined by

$$R(x,y) = R_0 e^{-\frac{(x-x_0)^2+(y-y_0)^2}{2d^2}} \quad (14)$$

where *R* is the rain rate, R_0 the maximum rain rate, x_0 and y_0 the rain cell center coordinates. *T*he 3 dB width, *d*, is defined so that the rain rate over the edge of the cell is only one hundredth of R_0.

$$d = r / \sqrt{2ln(100)} \quad (15)$$

The $\widetilde{\sigma_0}$ model defined by equation (12) can also be used with any analytical or measured rain rate field *R(x,y)*, such as the ones given by the Tropical Rainfall Mapping Mission (TRMM) rain radar or by a meteorological radar.

3 - Modeling results

The form of equation (12) shows that the modified NRCS, $\widetilde{\sigma_0}$, depends on the surface NRCS, σ_0, and on the attenuation and volume scattering within the rain cell. The surface NRCS itself depends on wind speed and azimuth, on incidence angle and on polarization. Before studying in section 3.2, the impact of rain on the quality of the wind retrieval by a scatterometer, which involves multiple surface NRCS measurements at different azimuths, incidence and polarizations, we first analyzed, in section 3.1, the effects of rain assuming a constant surface NRCS.

3.1 - Modification of NRCS

3.1.1 - $\widetilde{\sigma_0}$ within a rain cell. The $\widetilde{\sigma_0}$ fields are first computed using equation (12) at a 1 km horizontal resolution, i.e. a resolution similar to those of meteorological rain radars or the TRMM precipitation radar, over a square area twice the size of the rain cell radius. The surface NRCS is assumed constant.

As a scatterometer wind cell is typically of 25x25km² the 1 km resolution $\widetilde{\sigma_0}$ fields are averaged for each point *M (x,y)*, over 25x25 km² areas. These areas are also comparable to the Seawinds antenna footprint which is an ellipse of 24 km in azimuth and 31 km in the range direction for the inner beam and 26 km and 36 km for the outer beam (for a detailed description of the Seawinds system see for example, *[Spencer et al., 2000]*). The average NRCS is computed at every point of the 1km field because, as the effect of rain is strongly non-linear, the relative position of the rain cell and scatterometer resolution cell, i.e. the distribution

of rain within the scatterometer cell, can strongly impact the results.

For each point, the averaged rain rate R_{av}, averaged effective NRCS $\overline{\tilde{\sigma}_0}$, the standard deviation of NRCS $\sigma_{\tilde{\sigma}_0}$ are estimated by

$$R_{av}(x,y) = 1/N \sum_{i=1}^{N} R(x_i, y_i) \quad (16)$$

$$\overline{\tilde{\sigma}}_0(x,y) = 1/N \sum_{i=1}^{N} \tilde{\sigma}_0(x_i, y_i) \quad (17)$$

$$\sigma_{\tilde{\sigma}_0}(x,y) = 1/(N-1) \sqrt{\sum_{i=1}^{N} (\tilde{\sigma}_0(x_i, y_i) - \overline{\tilde{\sigma}}_0(x,y))^2} \quad (18)$$

where *i* represents the indices for the *N* 1km samples within the 25x25km² area.

Figure 4 (a to c) presents three examples of the $\tilde{\sigma}_0$ modeling for a 5 km height Gaussian rain cell of 15 km radius and maximum rain rate of 15 mm/hr and surface σ_0 of -5dB, -15 dB and -25dB. These values are representative of the range of possible NRCS measurements by Ku-band scatterometers (Seawinds and NSCAT). The sampling geometry corresponds to the Seawinds inner antenna configuration, 46° incidence and 70.3° azimuth. The 25 km averaged fields, $\overline{\tilde{\sigma}_0}$, are also presented in figure 4 (d to f).

For high σ_0 (>10 dB), corresponding to high winds, the surface NRCS is always attenuated, whatever the relative rain and scatterometer cells position. The maximum attenuation of 7dB is reached when the rain and scatterometer resolution cells centers are collocated. The averaging smoothes the field but the maximum attenuation still reaches 2.5dB. These values largely exceed the 10-15% radiometric resolution of the Seawinds sensor.

For medium σ_0, the $\tilde{\sigma}_0$ field presents a complex pattern of attenuation at far range and enhancement at near range where volume effects are predominant. Enhancement can reach 1.5 dB and attenuation -1.5 dB. The average field, $\overline{\tilde{\sigma}_0}$, presents a smoother pattern of enhancement and attenuation, with an amplitude of about ±0.5 dB. For a same rain cell, the net effect of rain will thus strongly depend on the relative position of the rain and scatterometer cell centers. For this particular rain cell and surface NRCS, the NRCS is not

modified if the two centers coincide. For low σ_0, i.e. low winds, the volume scattering is predominant everywhere and the signal is always enhanced. The contribution of the surface NRCS to the measured signal is almost negligible within the rain cell. The maximum enhancement exceeds 10dB at 1km resolution and 7dB at 25 km.

To quantify the importance of the partial beam filling , of the non-linearity of rain influence and of the rain-rate distributions within the rain cell, $\widetilde{\sigma_0}$ and $\overline{\widetilde{\sigma}_0}$ are also computed using equation (5) and assuming for each point *M(x,y)* an homogeneous layer of $R_{av}(x,y)$ rain rate. The resulting fields are presented in figures 5 a-b-c. This can be seen as an estimate of the rain correction that could be computed using a rain rate estimate from a sensor like the Special Sensor Microwave/Imager which has a resolution of about 30km. The difference between the 25km average $\overline{\widetilde{\sigma}_0}$ fields computed using equations (5) and (12) are also presented in figures 5 d-e-f.

The comparison of the two modeling results shows that the use of averaged rain rate tends to smooth and spread the NRCS correction. Both attenuation and volume scattering are underestimated within the cell. However, attenuation being not as strongly non linear as scattering, it is better represented by this simplified modeling. This can be seen for high σ_0, for which attenuation is predominant. The difference between the two models is weak and does not exceed 0.5dB (figure 5-d). This shows that for high winds a correction of the NRCS could be possible using coarse resolution rain rate fields such as those from SSM/I. *Yueh et al.* [2001] and *Stiles and Yueh* [2002] using collocated SSM/I rain rate measurements, NCEP wind fields and SeaWinds on QuikScat NRCS data, estimated that an empirical correction of scatterometer winds contaminated by light to moderate rain may be possible for winds greater than 5 m/s.. For medium σ_0, the complex pattern of attenuation and enhancement is not represented and only enhancement is present (figure 5b). The difference between the two $\overline{\widetilde{\sigma}}_0$ estimates varies from -.5dB to 1dB (figure 5e). For low σ_0, for which scattering is predominant, the difference between the two modeled $\overline{\widetilde{\sigma_0}}$ becomes important and varies, depending on the relative position of the rain cell and scatterometer cell, from -1 to +2.5dB (figure 5f).

These examples show the complexity of the problem of correction of rain effects on the NRCS. Indeed, the NRCS modification depends not only on the average rain rate within the scatterometer cell but also strongly on the distribution of rain within the cell. This can be a strong handicap to the correction of rain contamination if only low resolution rain rate fields are available.

They also show the importance of a good quantification of the modification of the NRCS by rain cells of different rain rates and diameters. Such a quantification is of prime importance to test and to improve the rain flagging procedures that have been developed for Seawinds.

3.1.2 - Modeling of $\widetilde{\sigma_0}$ for fixed surface NRCS and different rain cells. The effect of a large range of analytical rain cells, rain rate from 2 to 35 mm/hr and radius from 2.5 to 30 km, has been modeled for surface NRCS's covering the whole Seawinds range. For simplicity, the height of the rain cells has been fixed to 5 km, i.e. the mean freezing level altitude for the tropics. For each cell, $\widetilde{\sigma_0}$ is modeled at a 1 km resolution (as in figure 5) and the 25km averaged $\overline{\widetilde{\sigma_0}}$ is then computed. The maximum enhancement, $\Delta\overline{\widetilde{\sigma}}_{0max}$ and attenuation, $\Delta\overline{\widetilde{\sigma}}_{0min}$ are then determined. These two parameters correspond to the $\overline{\sigma_0}$ extremes in figures 4 d-e-f. Figure 6 presents both the $\Delta\overline{\widetilde{\sigma}}_{0min}$ (solid lines) and $\Delta\overline{\widetilde{\sigma}}_{0max}$ (dashed lines) fields for three rain rates, 4 mm/hr, 10 mm/hr and 25 mm/hr, for rain cell radius from 2.5 to 30 km and for surface σ_0 from -40 dB to -7.5 dB. Only the non null values of both parameters have been plotted in the figure.

For low σ_0 (<-25 dB), volume scattering is always predominant. The surface NRCS is always enhanced leading to a an overestimation of the wind speed. For rain rates greater than 4 mm/hr and radius larger than 10 km, the increase of NRCS is always larger than 5 dB. For σ_0 between -25 dB and -12.5 dB, the effect of rain depends quite strongly on the relative position of the rain and scatterometer cell centers as in the case presented in figure 4b. Both attenuation and enhancement can occur . However, attenuation is an order of magnitude smaller than the enhancement and exceeds 1 dB only for high rain rates . For high σ_0 (>-10 dB), attenuation becomes predominant but, except for high rain rates (>10 mm/hr) and large radius (>10 km) it is less than 2 dB.

In all cases, for rain rates greater than 10 mm/hr and radii greater than 10 km, the modification of the NRCS is so important that no pertinent information on the surface σ_0 could be retrieved without a precise knowledge of the rain rate field within the scatterometer cell.

One of the parameters which can be computed from scatterometer data to help to identify rain contamination is the variability of NRCS within a resolution cell. For example, a Seawinds cell may contain between 12 to 45 composite σ_0 measurements, depending on the cell cross-track position. The linear standard deviation $\sigma_{\widetilde{\sigma_0}}$ computed from the model gives an estimate of the NRCS variability induced by the presence of a rain cell within a scatterometer cell. For each rain cell and surface NRCS, the maximum $\sigma_{\widetilde{\sigma_0}}$ has been

determined using equation (18) . The resulting fields are presented in figure 6(d to f). As expected the $\sigma_{\widetilde{\sigma_0}}$ strongly increases with rain rate and decreases with surface NRCS. The NRCS variability tends to decrease for large rain cell radii for which the rain rate gradients within a scatterometer resolution cell becomes smaller.

For low σ_0, $\sigma_{\widetilde{\sigma_0}}$ is always very large even for low rain rates and small radii. This shows that a rain flag based on the surface NRCS variability within a scatterometer cell can perform well for low wind speeds. For medium and high σ_0, the problem becomes more complex as $\sigma_{\widetilde{\sigma_0}}$ remains relatively small even for high rain rates. This is particularly true for small intense rain cells.

3.1.3 -Variation of NRCS as a function of average rain rate. The previous sections show that the NRCS modification by rain cells is a complex phenomenon which depends on several parameters: sensor sampling geometry (incidence, azimuth), rain cell characteristics (rain rates, radius), surface NRCS and relative position of the rain cell and scatterometer resolution cell centers. The correction of scatterometer measurements in presence of rain appears difficult, except if coincident high resolution rain data are available. In regard to the results of the rain influence modeling using 25km average rain rate fields, even a efficient rain flag validation, except for high rain rates, using data such as the ones from SSM/I appears problematic.

However, it is important, at least for a better rain flagging, to have an estimate of the mean NRCS change as a function of the average rain rate over a scatterometer cell. Such estimates can be used to give a confidence level to inverted wind vectors if, for example, coincident passive microwave rain rate estimates are available.

Using the model results of section 3.1.2, for each rain cell of rain rate R_0 and radius *r*, the averaged rain rates, R_{av}, are computed, as well as the 25 km resolution modified NRCS $\overline{\widetilde{\sigma}_0}$. For each R_{av}, the mean NRCS modification, $\Delta\overline{\widetilde{\sigma}_0}$, are computed. The results are then averaged over the whole range of rain cell rates and radius. Figure 7-a presents the mean $\Delta\overline{\widetilde{\sigma}_0}$ for different mean rain rates as a function of the surface NRCS. The shape of the curves is similar to the ones presented in figure 2-b for which homogeneous rain layers and a simplified model of equation (5) were used. However, the difference of NRCS between the two models can reach several dB's (figure 7-b). For low NRCS, the scattering is underestimated whilst the attenuation is underestimated for high NRCS. For medium NRCS for which the two effects have similar importance, the difference between the models depends strongly on rain rate with an inversion of behavior

near -10 dB.

3.2 - Influence on wind retrieval

3.2.1 - Wind retrieval within a rain cell. When considering wind retrieval, the problem of rain becomes even more complex. Indeed, as shown in section 3.1, the effect of rain strongly depends both on the surface backscatter and on the relative position of the scatterometer and rain cell centers. As the wind retrieval from scatterometer data over a sensor resolution cell is based on a set of NRCS measurements at different azimuths and incidence angles, different polarizations and in different individual beam measurements located within the retrieval cell, the modification of NRCS for each of the individual measurement can be very different.

For Seawinds, this effect is tested in following manner. For consideration of the azimuth, incidence angle and polarization diversity, only four σ_0 are required to process the wind vectors as in the Seawinds configuration: two σ_0 at opposite azimuths (see Appendix A) for the inner and outer antennae which have different incidence angle and polarization.

The surface wind is assumed constant, within the rain cell. This is certainly not true for real cases as rain cells might commonly be associated with inhomogeneous wind fields but this assumption allows to better understand the effect of rain on the wind retrieval. The four associated surface NRCS are then estimated using the KMOD model function *[Wentz and Smith, 1999]*. The effective NRCS $\widetilde{\sigma}_0$ are then modeled at a 1 km resolution using equation (12) and averaged over 25 km cells. The resulting $\overline{\widetilde{\sigma}}_{0i}$ are inverted in terms of wind speed and direction using the KMOD model function and a maximum likelihood estimator *[Quilfen and Cavanié, 1991]*.

Figure 8 presents an example of the modification of surface NRCS, $\Delta\overline{\widetilde{\sigma}}_{0i}$, produced by a 5 km height Gaussian rain cell of 15 km radius and 15 mm/hr for a constant surface wind of 10 m/s and 60° direction. The rain cell center is located 300 km from the satellite track. In this particular case, the azimuths ψ for the inner and outer antennae are respectively ± 70.3° and ± 75.94°. The effective surface NRCS using the KMOD model function, are about -21 dB and -20 dB for the inner antenna and -18.3 dB and -16.7 dB for the outer antenna. These differences of surface backscatter and incidence angle produces strong variations of the modification of NRCS by rain. It exceeds 4.5 dB for the inner antenna and it is less than 1dB for the outer antenna.

The differential effect of rain on the 4 σ_0's strongly hamper the wind vector retrieval as it can be seen in figure 9-a which presents the winds retrieved from the 4 rain modified $\widetilde{\sigma}_0$ of figure 8. Depending on the relative position of the rain and scatterometer cell centers, the wind speed error can reach 7 m/s and the wind direction error 60°. From figure 9-a, it is obvious than the same average rain rate within a scatterometer resolution cell can result in very different modifications of the retrieved wind vector, depending on the distribution of rain within the cell.

Figure 9-b and c which present the scatter plots of wind speed and direction, respectively, as a function of the averaged rain rate $R_{av}(x,y)$ defined by equation (16), show that even for average rain rate as low as 2 mm/hr, the wind speed and direction errors can be as large as 5 m/s and ±60°. The dispersion of the errors, i.e. the influence of the relative position of the rain cell and scatterometer cell centers, increases for low rain rates and is about 5 m/s and 120° for 2 mm/hr.

As already presented in section 3.1.1 for a constant surface NRCS, the potential correction of the influence of rain using low resolution rain rate data (such as the SSM/I ones) has also been tested assuming within each 25x25 km² cell a constant and homogeneous rain layer of R_{av} rate and the model described by equation (5). The rain modified NRCS have been computed for the two antennae and azimuths and have then been inverted in the same way as previously. The resulting wind field and scatter plots are presented in figure 9 (d to f).

Using such modeling, a possible correction for a 2 mm/hr rain rate would be in this particular case (10 m/s, 60° wind, rain cell located 300km off the satellite track), 3 m/s and 30°. However, the comparison with the full resolution modeling shows that the wind speed error is overestimated (by 1 to 3 m/s) near the rain cell center and underestimated near the rain cell edges (by 1 m/s). The difference of wind direction error can reach 60° and has a complex pattern, being more important where large gradient of rain rate are present (near the rain cell edges for example) and small where the rain rate field is smoother (near the rain cell center). The dispersion of the errors results only in a slight variation of surface NRCS as a function of the position *(x,y)* and is largely underestimated compared to the full resolution modeling.

The distance between the modified NRCS and the surface NRCS constitutes an other approach to the quantification of the effect of rain. This distance, which is also used as a maximum likelihood estimator for the estimation of the best retrieved wind vector, is computed by

$$MLE = \frac{1}{N}\sqrt{\sum_{i=1}^{N}\frac{(\widetilde{\sigma}_{0i} - \sigma_{0i})^2}{k_p \sigma_{0i}}} \quad (19)$$

where k_p is the radiometric resolution of the sensor *[Quilfen and Cavanié, 1991]*.

Two MLE fields are computed, first, between the rain modified NRCS, $\overline{\widetilde{\sigma}_0}$, and the true surface one, σ_0, and secondly between $\overline{\widetilde{\sigma}_0}$, and the KMOD NRCS, σ_0^{mod}, retrieved during the wind inversion process. The first MLE give the measure of the distance introduced by rain from the true NRCS and the second one gives an estimate of what an operational inversion process would recover (distance to the KMOD model). The two fields, presented in figure 10, shows that even though the distance introduced by rain is in general large and exceeds the threshold value generally used for quality flagging, the MLE of the inversion is always very low, because it is the purpose of the inversion to minimize the MLE and thus large errors in NRCS can result in values relatively close to KMOD, but for wind speed and direction values far from the truth. This shows that a rain flag based only on simple MLE estimates can hardly properly function.

3.2.2 - Wind retrieval errors as a function of rain cell characteristics. To generalize the results of figure9 and as the surface NRCS strongly varies with wind vector, the modification of the retrieved wind vector for different wind speeds as a function of the rain rate and rain cell diameter are computed. Figure 11 presents the retrieved wind vector for 3 surface wind vectors (5, 10 and 25 m/s, 60° direction) as a function of rain cell characteristics (rate and radius). For each rain cell, the wind has been inverted for the location where the distance induced by rain from the KMOD model is maximum.

For low and medium winds (5 m/s, 10 m/s), the wind speed will be overestimated and the overestimation can largely exceeds 10 m/s for high rain rates. Except for very small rain cells, the wind direction is severely modified. For medium wind, the wind speed is underestimated for low rain rates and small diameter and overestimated for rain rate higher than 10 mm/hr and 10 km. For higher winds, the wind speed is slightly overestimated for low rain rates and small diameter and underestimated elsewhere. The error remains small (<2 m/s). However, as for lighter winds, the wind direction is strongly modified for rain rates higher than 10 mm/hr.

3.2.3 - Wind retrieval errors as a function of average rain rate. The above model results can also be presented in another way which emphasized the mean impact of the average rain rate within a scatterometer cell. As for constant surface NRCS, the errors on wind speed and direction have been computed as a function

of average rain rate for a large range of rain cell. The results of this modeling are presented in figure 12. The effect of rain on retrieved wind speed is, as expected from the form of the KMOD model function, very similar to the one on the NRCS. For wind speed lower than 22 m/s, the wind speed is overestimated. The error increases with rain rate and true surface wind speed and exceeds 5m/s for rain rates higher than 5 mm/hr and wind speed lower than 15 m/s.

For wind speed around 20-22 m/s, attenuation and volume scattering by rain tend to compensate and the wind speed error remains small (<1 m/s) even for high rain rates. For high winds, the speed is underestimated by up to 10 m/s for 30m/s winds and 25 mm/hr rain.

The effect on wind direction strongly depends, as shown in section 3.2.2, on the distribution of rain within the scatterometer resolution cell and is thus more complex than the one on wind speed. The mean error is thus weakly dependent on true wind speed and rain rate and remains quite small (around ±20°) for wind speed above 10 m/s. It slightly increases to 30-40° for 5 m/s winds. However, the dispersion around these mean relations is much larger (~40°) than the mean itself, which considerably reduces their significance. The wind direction error almost behaves like a random variable and no correction can possibly be applied using only averaged rain rates.

4 - Comparison with the ERS AMI-Wind C-band scatterometer

The model described in section 3 has also been used to analyze the influence of rain on the AMI-Wind C-band scatterometer data. At this band, attenuation and scattering are one order of magnitude smaller than at Ku-band. The modification of NRCS is noticeable only for rain rates higher than 5 mm/hr. For 10 mm/hr rain, attenuation is still lower than 0.2 dB and enhancement lower than 1.5 dB. For AMI-Wind, the wind retrieval will only be affected by medium to high rain rates. Figure 13 presents the results of the same modeling as the one presented in section 3.2.3 (figure 12) for Seawinds. For wind speeds lower than 15 m/s and rain rates lower than 15 mm/hr, the wind speed error remains below 1 m/s and the wind direction below 15°. For high rain rates (above 20 mm/hr), the speed of high winds (>20 m/s) is underestimated by more than 2 m/s whilst the direction of low winds is off by 20°.

For AMI-Wind, the atmospheric effects of rain, despite for high rain rates, can be considered as negligible on the quality of the wind retrieval. Such conditions can be encountered for example in tropical cyclones or in

squall lines.

5 - Conclusions and perspectives

The impact of rain cells on scatterometer backscatter measurements is complex as scattering and attenuation by rain drops have opposite impacts on the measured NRCS and the quality of wind vector estimates can be severely altered even for low rain rates. Using a simplified cylindrical Gaussian rain cell model, and some simplifying approximations, a numerical model of computation of the effective NRCS in presence of a rain cell has been developed .

The modeling results at Ku-band, assuming a constant surface NRCS, show that scattering by rain drops plays a major role at low NRCS, resulting in a signal enhancement, and that attenuation predominates for high NRCS. Even rain rates as low as 1 mm/hr can significantly modify the NRCS (up to 10 dB). The analysis of modified NRCS within rain cells points out that it depends more strongly on the distribution of rain within the scatterometer resolution cell than on the average rain rate within the cell. This implies that a correction of NRCS using for example SSM/I type rain rates estimates can not performed correctly and that high resolution rain fields, such as the one given by the TRMM precipitation radar, are required. This is also confirmed by the comparison of the NRCS modifications computed by the full resolution model with a simple one assuming a constant homogeneous rain layer filling the scatterometer cell. These results also suggest that even the validation of rain flags for low rates, especially the determination of the proportion of false alarm, using SSM/I data would be difficult.

The analysis of NRCS variance within a scatterometer cell shows that this parameter is highly sensitive to the presence of rain especially for low NRCS. This suggests that an estimate of the NRCS variability, based for example in the case of Seawinds on the slice measurements could be a possible candidate for a rain flag.

The influence of rain on the wind retrieval on the Seawinds configuration has also been modeled. As the influence of rain strongly depends on the surface NRCS, the effect on the retrieved wind vectors, which involves measurements at different incidences, azimuths and polarization is even more complex than in case of constant surface NRCS. Because of the shape of the KMOD model function, the error induced by rain on wind speed follows a similar trend as the one on NRCS, i.e. an overestimation of low winds and an

underestimation of high winds. For winds near 20 m/s, attenuation and volume scattering tend to compensate and the error to cancel . The wind direction is affected in a more complex manner and depends more strongly on the rain rate distribution within the scatterometer resolution cell than any other parameter (average rain rate, wind speed). No general trend can really be discerned and the dispersion around the mean values is so high that the retrieved wind direction can be considered as a random variable.

For a given wind vector, the NRCS modification by rain moves the set of backscatter measurements used in the inversion process far away from the KMOD model function. The distance induced is always large, even for low rain rates. However, because this difference between true and modified NRCS's is compensated by modifying the speed and direction of the wind during the inversion process, the MLE value obtained remains relatively low and in most of the cases within acceptable limits. This makes the MLE hardly suitable for rain flagging, even though a more sophisticated MLE based algorithm used in the Seawinds products shows some skill *[Mears et al., 1999]*.

The model has also been used to test the influence of rain on the C-band AMI-Wind instrument. At this band, attenuation and scattering are one order of magnitude lower than at Ku-band. As expected the modification of NRCS by rain becomes only a problem for high rain rates and high winds. For average rain rates below 20 mm/hr the model does not point out any alteration of retrieved wind vectors larger than 1 m/s and 15°.

The results of this study shows that Ku-band scatterometer data are greatly affected by rain and extremely sensitive to the rain distribution within a scatterometer resolution cell. Even low rain rates can seriously modified the retrieved wind vectors. This confirms that good rain flagging is still an important issue for the operational use of Ku-band scatterometer data. The theoretical analysis here shows that for rain rates over 5 mm/hr the modification of backscatter is so important and complex that the availability of high resolution rain data can significantly improve efficient correction of rain contaminated scatterometer cells, particularly for low and moderate wind speeds.

Appendix A: Sampling geometry of the ocean surface by a scatterometer

Two types of scatterometers have been or are currently flown on satellites. The first type has two or three fixed antennae looking at different fixed azimuth angles, and covering different incidence angles. This kind of instrument have been used on Seasat, ERS-1 and ERS-2 (AMI-Wind instrument) and on ADEOS-1 (NSCAT). The second kind has two rotating antennae at fixed incidence angles. Such an instrument is currently flown on board the QuikScat satellite and a similar one will be flown on ADEOS2.

Depending on the type of scatterometer, the influence of a rain cell on the wind retrieval will be quite different. Indeed, as shown in figure2, the effect of rain strongly depends on the surface NRCS, which itself depends, for a given surface wind vector, on azimuth, incidence and polarization.

Rotating antennas scatterometer (QuikScat): The Seawinds scatterometer operates at Ku-band (13.46 GHz), it uses a 1-meter-diameter rotating disk that produces two spot beams, sweeping in a circular pattern. The incidence angles, ϕ , are respectively 46° and 54° for the inner and outer beams. Within a wind retrieval resolution cell (25x25 km²), a point M of the sea surface will be sampled by each antenna under two different azimuths ψ and $-\psi$. This azimuth angle is determined by the position of the satellite and the incidence angle.

Taking into account the earth curvature, the ground range distance, r_a, is given by

$$r_a = \frac{H}{\cos(\phi)} + H\frac{^2}{2a}\tan^2(\phi) \quad \text{(A.1)}$$

where *H* is the satellite altitude, *a* the earth radius and ϕ the incidence angle. The azimuth angles of a point *M (x,y)* are defined by

$$\psi = \pm\arccos(y/r_a) \quad \text{(A.2)}$$

where *y* is the cross track distance of *M*.

Fixed antennas scatterometer (ADEOS-1, ERS): NSCAT and AMI-WIND scatterometers are three antennae instruments operating at Ku (14 GHz) and C-band (5.6 GHz) respectively. The antennae azimuth are respectively 45°, -25° and -45° for NSCAT and 45°, 0°, -45° for AMI-WIND. NSCAT has two 600 km wide swaths, located on each side of the satellite track, separated by 300 km. AMI-WIND has one 500 km wide swath located 250 km off the right side of the satellite track.

Each point of the rain cell will be sampled by each of the three antennae at fixed azimuth but at different

incidence angles. For each antenna, the intersection of the beam and the rain cell are computed as well as the incidence for each point affected by rain. The range and incidence under which a point *M (x,y)* will be seen are given by

$$s = \frac{y}{\cos(\phi)}$$
$$\phi = \arctan\left(s/\left(H + \frac{x^2}{2a^2\cos^2(\psi)}\right)\right) + \arcsin(s/a) \quad \text{(A.3)}$$

where ψ is the antenna azimuth angle, *y* the across track distance, and *a* the earth radius.

References

Bliven L. F., and J. P. Giovanangeli, An experimental study of microwave scattering from rain- and wind-roughened seas, *Int. J. Remote Sensing*, **14**, 2315-2329, 1993.

Capsoni, C, F. Fedi, C. Magistroni., A. Paraboni, and A. Pawlina,, Data and theory for a new model of the horizontal structure of rain for propagation application, *Radio. Sci.*, **22**, 395-404, 1987.

Craeye C. and P. Schlüssel, Rainfall on the sea: surface renewals and wave damping, *Bound. Layer Met.*, **89**, 349-355, 1998.

Doviak, R.J. and D.S. Zrnic, *Doppler Radar and Weather Observations*, Academic Press,1984.

Goldhirsh, J., and B. Musiani, Rain cell size statistics derived from radar observations at Wallops Island, Virginia, *IEEE Trans. Geosci. and remote Sensing*, **24**, 947-954, 1986.

Guymer, T. H., J. A. Businger, W. L. Jones, and R. H. Stewart, Anomalous wind estimates from Seasat scatterometer, *Nature*, **294**, 735, 1981.

Huddelston J.N. and B.W. Stiles, *Multidimensional histogram (MUDH) rain flag*, Jet Propulsion Laboratory, California Institute of Technology , 2000.

Marshall, J.S. and W. McK. Palmer, The distribution of raindrops with size, *J. Meteor.*, **5**, 165-166, 1948.

Mears C., F. Wentz, and D. Smith, *Special Product: Sea Winds on Quikscat normalized objective function*, Remote Sensing System, Santa Rosa, Ca., 1999.

Melsheimer, C. , W. Alpers, and M. Gade, Investigation of multifrequency/multipolarization radar signatures of rain cells over the ocean using SIR-C/X-SAR data , *J. Geophys. Res.*, **103**, 18,851-18,866, 1998.

Moore, R.K., A.H. Chaudry, and I.J. Birrers, Errors in scatterometer-radiometer wind measurements dur to rain, *IEEE J. Ocean. Eng.*, **OE-8**, 37-49, 1983.

Moore, R.K., I.J. Birrer, and E.M. Bracalante, Evaluation of atmospheric attenuation from SMMR brigthness

temperature for the Seasat satellite scatterometer, *J. Geophys. Res.*, **87**, 3337-3354, 1982.

Olsen R. L., D. V. Rogers, and D. B. Hodge, The aRb relation in the calculation of rain attenuation, *IEEE Trans. Antennas and Propag.*, **AP-26**, 318-329, 1978.

Quartly G. D., Understanding the effects of rain on radar altimeter waveforms data:Part I: Theory, *J. Atmos. Ocean. Technol.*, **15**, 1361-1378, 1998.

Quilfen, Y., and A. Cavanié, A high precision wind algorithm for the ES1 scatterometer and its validation, *Proc. IGARSS 1991, Espoo, Finland*, 873-876, 1991

Quilfen Y., B. Chapron, T. Elfouhaily, K. Katsaros, and J. Tournadre, Structures of tropical cyclones observed by high resolution scatterometry, *J. Geophys. Res.*, **103**, 7.767-7.777, 1998.

Slack, J. K., A.R. Holt, and V. Brown, WP 400 Workpackage, Implementation of direct algorithms,*Rain radar retrieval algorithms*, Ed. by J. Testud, 1994

Smith, D.K. and F. Wentz, Correction of rain affected NSCAT winds, *Proc. of 1998 Fall AGU Meeting*, , 1998

Sobieski P., C. Craeye, and L. F. Bliven, Scatterometric signatures of multivariate drop impacts on fresh and salt water surfaces, *Int. J. Remote Sens.*, **20**, , 1999.

Spencer, M.W., C.L. Wu, and D.G. Long, Improved resolution backscatter measurements with the SeaWinds pencil-beam scatterometer, *IEEE Trans. Geosci. Rem. Sens.*, **38**, 2642-2652, 2000.

Spencer M. and M. Shimada, Effect of rain on Ku-band scatterometer wind measurements, *Proc. Conference IGARSS'91*, **Vol. II**, 1285-1287, 1991.

Stiles, B. W. and S. H. Yueh, Impact of rain on spaceborne Ku-Band Wind scatterometer, *IEEE Trans. Geosci. Remote Sensing*, **40-9**, 1973-1983, 2002.

Tournadre J., Determination of rain cell characteristics from the analysis of TOPEX, *J. Atmos. Ocean. Technol.*, **15**, 387-406, 1998.

Ulaby, F. T., R. K. Moore and A. K. Fung, *Microwave remote sensing: fundamentals and radiometry*, Artech

House, Norwood, Mass.,1981.

Wentz, F. J., and D. K. Smith, A model function for the ocean-normalized radar cross section at 14 GHz, *J. Geophys. Res.*, **104**, 11,499-11514, 1999.

Yueh S.H., B. Stiles, W.Y. Tsai, H. Hua and W.T. Liu, QuickSCAT Geophysical model function for tropical cyclones and application to hurricane Floyd , *IEEE Trans. Geosc. Remote Sens.*, **39**, , 2001.

Figure captions

Figure 1 : Radiation transfer across an infinitesimal cylinder

Figure 2 : (a) Effective normalized radar cross section at Ku-band ($\widetilde{\sigma}_0$) (solid lines) at 46° incidence angle as a function of rain rate for σ_0 from -35 dB to 5 dB assuming the scatterometer resolution cell is completely filled by homogeneous 5km height rain layer. The dashed lines represents the case where only attenuation is considered and the heavy dashed line the rain volume scattering. Typical surface NRCS values for the Seawinds scatterometer are between -35dB and -10dB.(b) Modification of effective NRCS as a function of NRCS for different rain rates.

Figure 3 : (top) rain cell geometry in the (y,z) plan. The light gray area represents the rain cell and the dark gray area the volume contributing to the signal at range y. (bottom) Cylindrical rain cell geometry in the (y,z) plan.

Figure 4 : Variation of NRCS induced by a 7.5 km radius Gaussian cylindrical rain cell of 25 mm/hr maximum rain rate and 5 km height . The incidence angle is 46° (Seawinds inner antenna), and the azimuth is 70.3° (indicated by the solid arrow). (i.e. rain cell located at y=300 km). The 1km resolution fields, $\widetilde{\sigma}_0$, are presented on the top panels for surface σ_0 of (a) -5dB, (b) -15dB, (c) -25dB, respectively. The corresponding 25x25km^2 averaged NRCS field $\overline{\widetilde{\sigma}_0}$ are presented on the bottom panels (d to f). For a better legibility, attenuation is associated to dashed lines and enhancement to solid lines.

Figure 5 : Variation of NRCS induced by a 25x25km^{2}averaged rain field corresponding to the rain cell of figure 4 The 25x25km^2 resolution fields $\overline{\widetilde{\sigma}_0}$ are presented on the top panels for surface σ_0 of (a) -5dB, (b) -15dB, (c) -25dB. The bottom panels (d to f) present the difference between the average NRCS fields of the top panels and those of figure 4-d to 4-f.

Figure 6 : Maximum NRCS attenuation, $\Delta\overline{\widetilde{\sigma}}_{0max}$ (dashed lines) and enhancement $\Delta\overline{\widetilde{\sigma}}_{0min}$ (solid lines) as a function of surface NRCS and rain cell radius for three rain rates: (a) 4 mm/hr, (b) 10 mm/hr and (c) 25 mm/hr. Only the non null values of both parameters have been plotted. The corresponding linear standard deviation, $\sigma_{\widetilde{\sigma}_0}$, are presented in the bottom panels (d to f).

Figure 7 : (a) Mean variation of NRCS as a function of surface NRCS for average rain rate of 1 to 25 mm/hr. The triangles represent ±1 standard deviation around the mean curves. (b) Difference between

the modified NRCS estimated using equation (5) (see figure 2.b) and the ones presented in (a).

Figure 8 : 25x25km^2 averaged rain modified NRCS for the Seawinds inner antenna , azimuth (a) +70.3°, (b) -70.3°, and the outer antenna, azimuth, (c) +76°, (d) -76°. The rain cell characteristics are: 5 km height, 15 km radius, and 15 mm/hr rate. The surface wind is assumed constant at 10 m/s and 60°.

Figure 9 : Top panels: (a) Retrieved wind speed isolines and wind vectors from the surface NRCS of fig. 8. Only one vector out of 5 in each direction is represented. The lower left corner arrow represents the underlying wind field (10m/s, 60° direction). Scatter plots of average rain rate over 25x25km² cells, R_{av} , and (b) retrieved wind speed, (c) wind direction. Bottom panels: Same as top panels but assuming a constant rain layer of R_{av} rate over the 25x25km² scatterometer cells.

Figure 10 : (a) Distance between the rain modified NRCS, $\overline{\widetilde{\sigma}_0}$, and the true surface NRCS, (b) maximum likelihood estimator values of the inverted $\overline{\widetilde{\sigma}_0}$.

Figure 11 : Influence of rain rate and rain cell radii on the wind retrieval for different constant wind vectors, (a) 5 m/s and 60°, (b) 10 m/s and 60°, (c) 25 m/s and 60°. The isolines of the retrieved wind speed at the center of rain cell are plotted as solid lines. Wind vectors are plotted as arrows and the lower left corner one represents the constant wind vector.

Figure 12 : Mean influence on (a) wind speed and (b) wind direction of average rain rate within a scatterometer cell as a function of true surface wind speed. The triangles represent ±1 standard deviation around the mean curves.

Figure 13 : Mean influence on (a) wind speed and (b) wind direction of averages rain rate within a scatterometer cell as a function of true surface wind speed for the C-band AMI-Wind instrument. The triangles represent ±1 standard deviation around the mean curves.

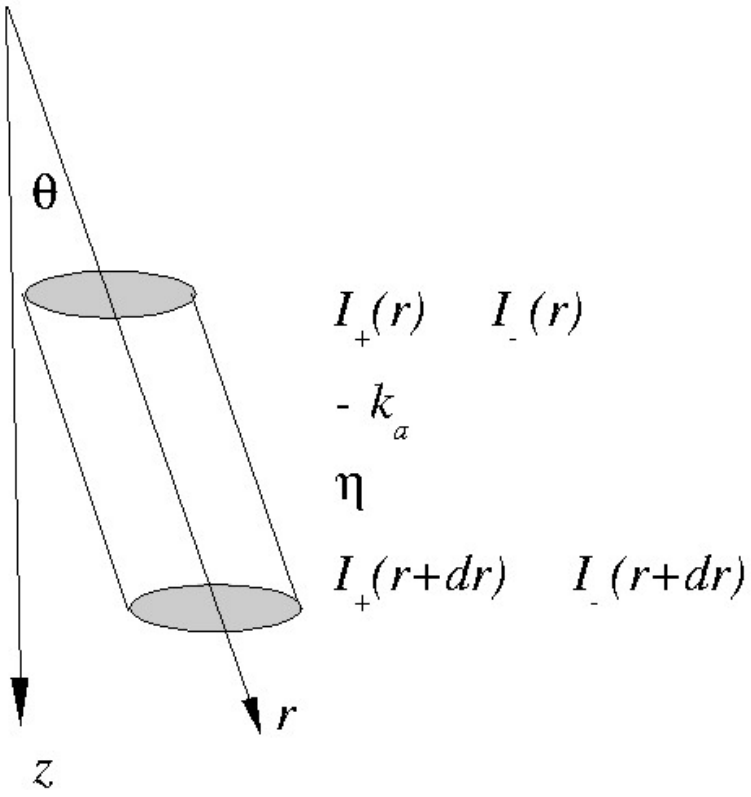

Fig. 1

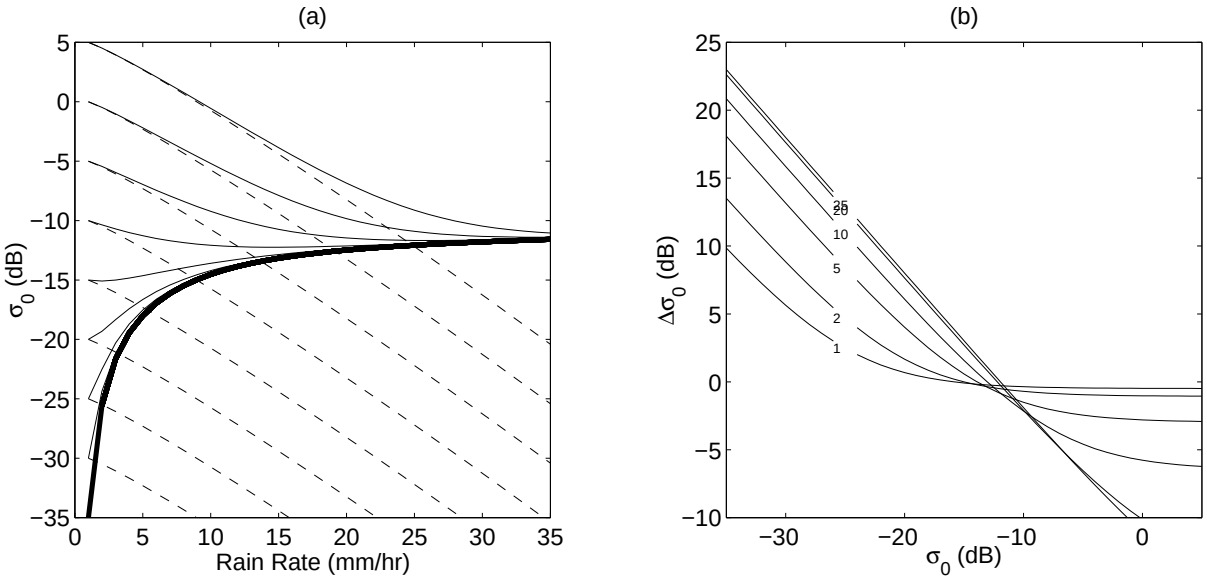

Fig2

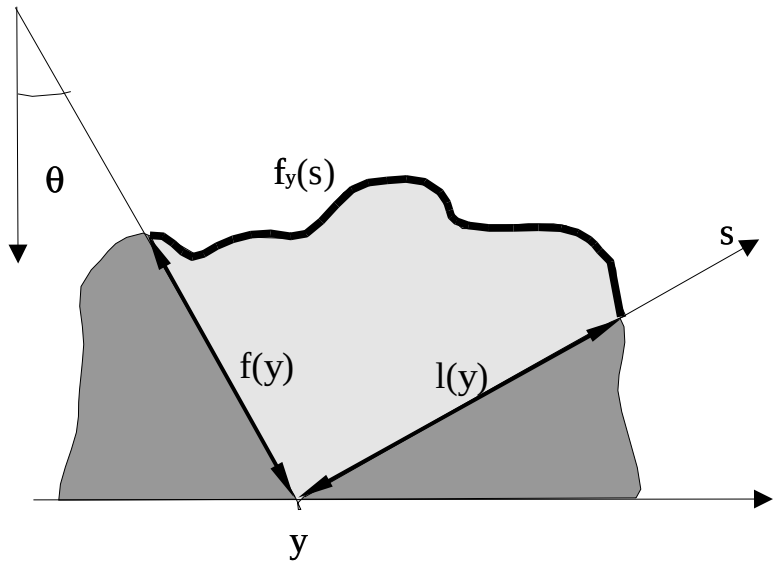

Figure 3(a)

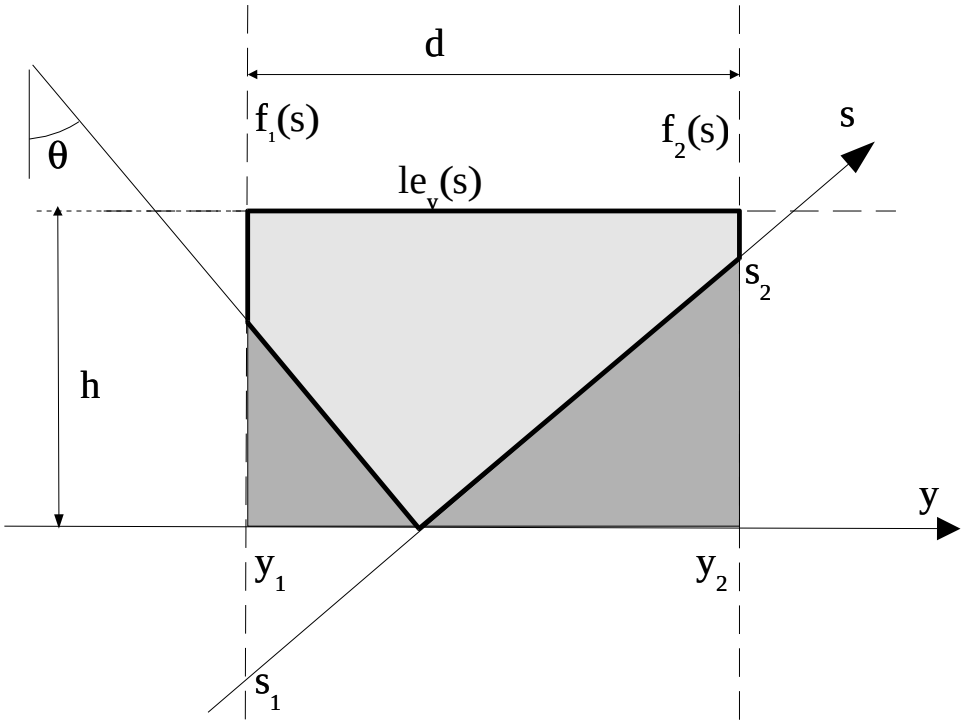

Figure 3 (b)

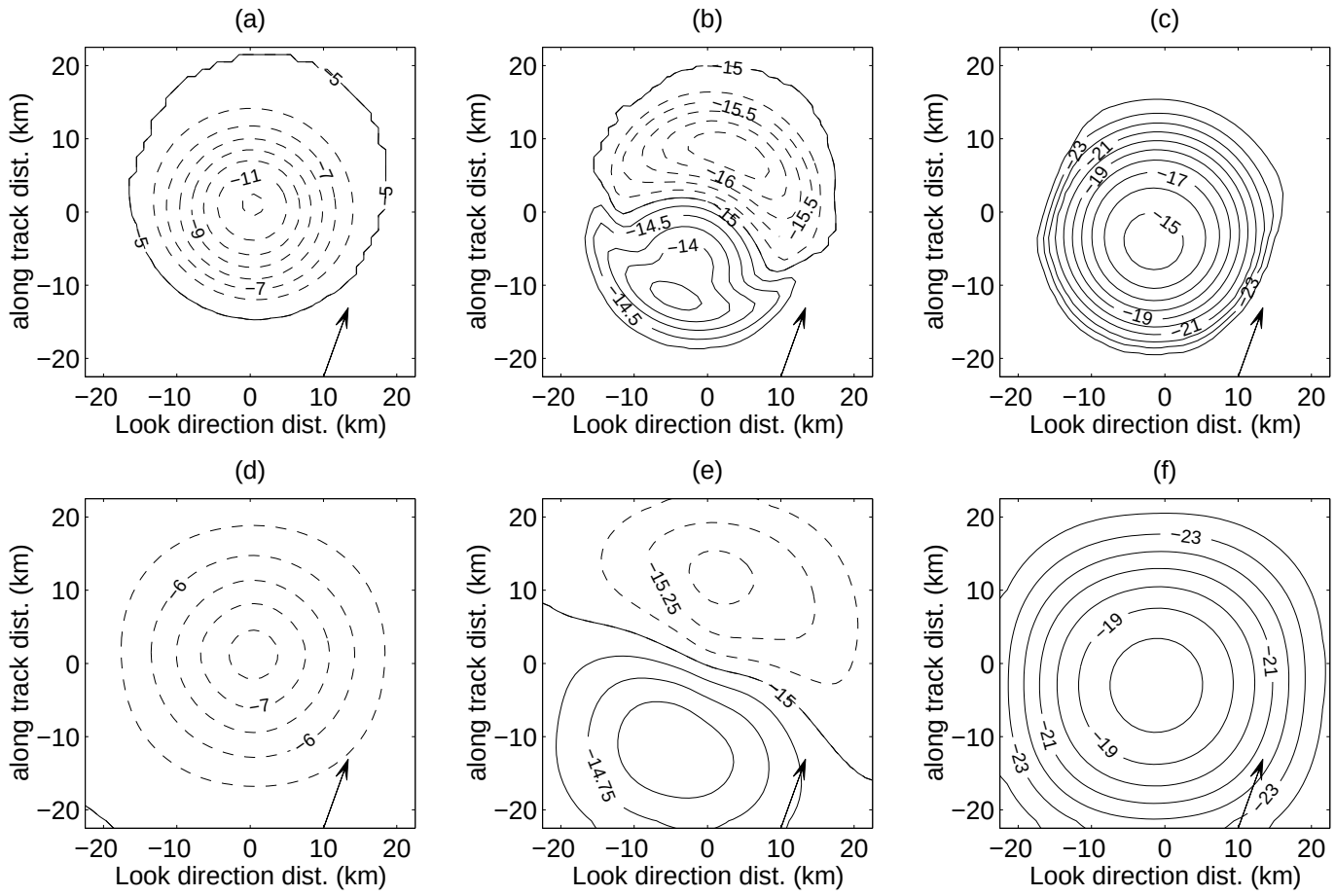
(a)
(b)
(c)
(d)
(e)
(f)
along track dist. (km)
Look direction dist. (km)
20
10
0
−10
−20
−20
−10
0
10
20
−5
−7
−9
−11
−15
−15.5
−16
−14.5
−14
−15.5
−23
−21
−19
−17
−15
−6
−7
−15.25
−15
−14.75
−23
−21
−19

Fig. 4

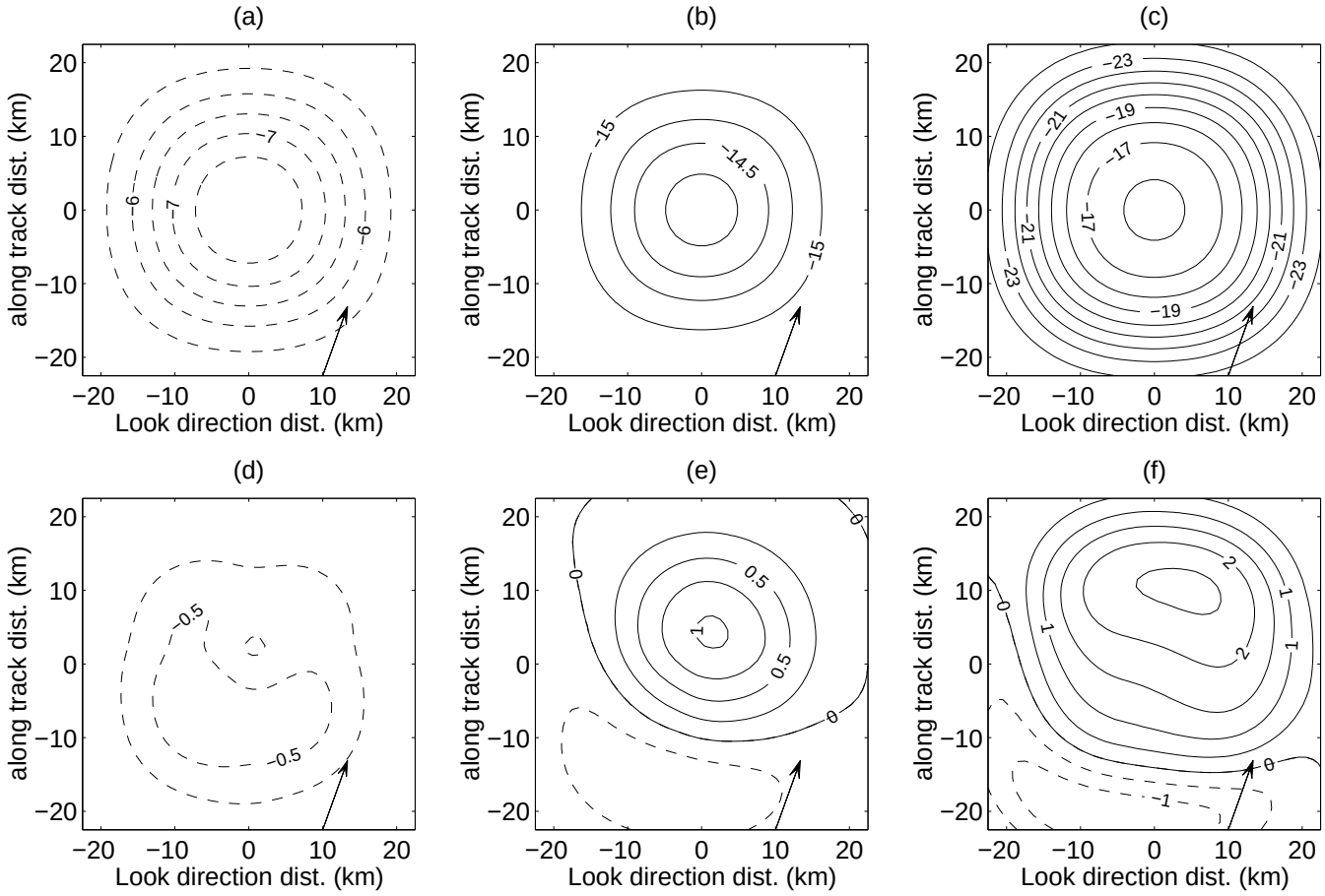
(a)
(b)
(c)
(d)
(e)
(f)
along track dist. (km)
Look direction dist. (km)
−20
−10
0
10
20
−7
−6
−15
−14.5
−23
−21
−19
−17
−0.5
0.5
1
2

Fig 5

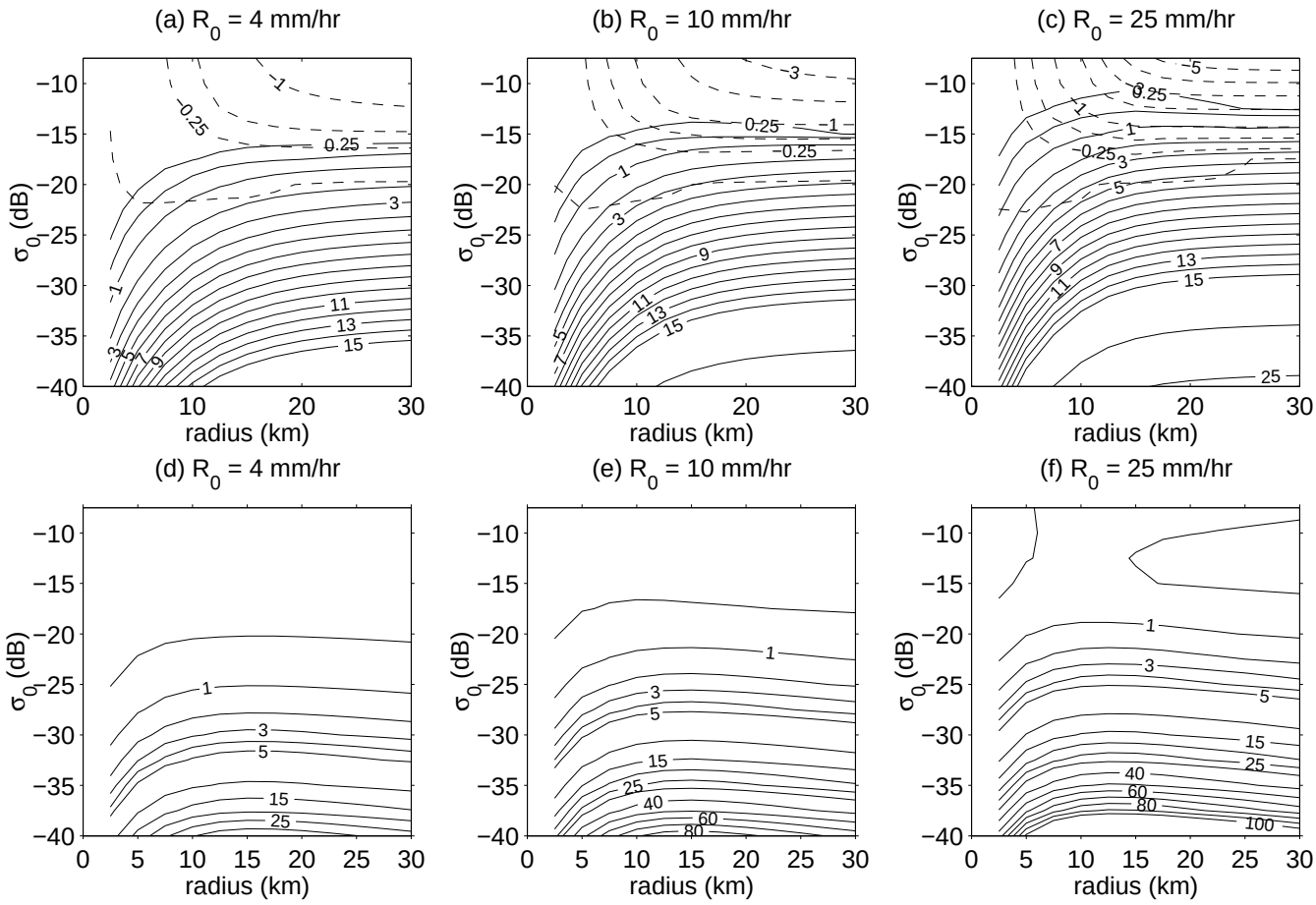
(a) R0 = 4 mm/hr
(b) R0 = 10 mm/hr
(c) R0 = 25 mm/hr
(d) R0 = 4 mm/hr
(e) R0 = 10 mm/hr
(f) R0 = 25 mm/hr
σ0 (dB)
radius (km)

Fig 6

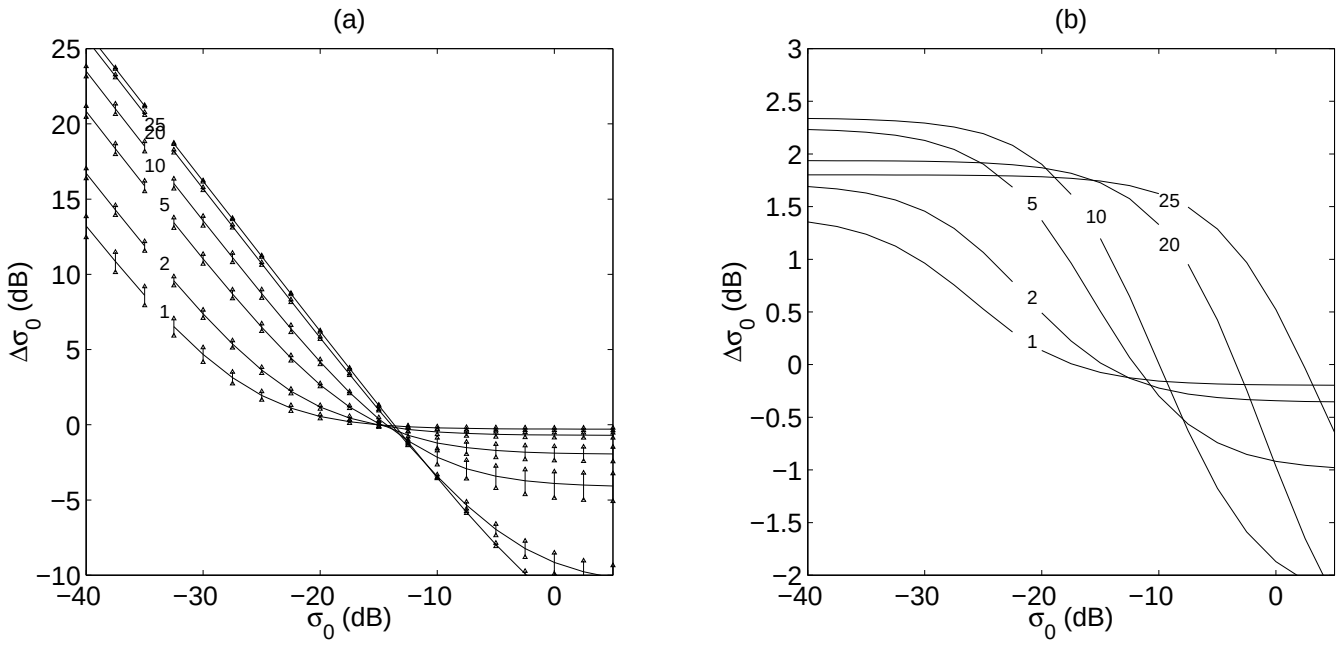

Fig 7

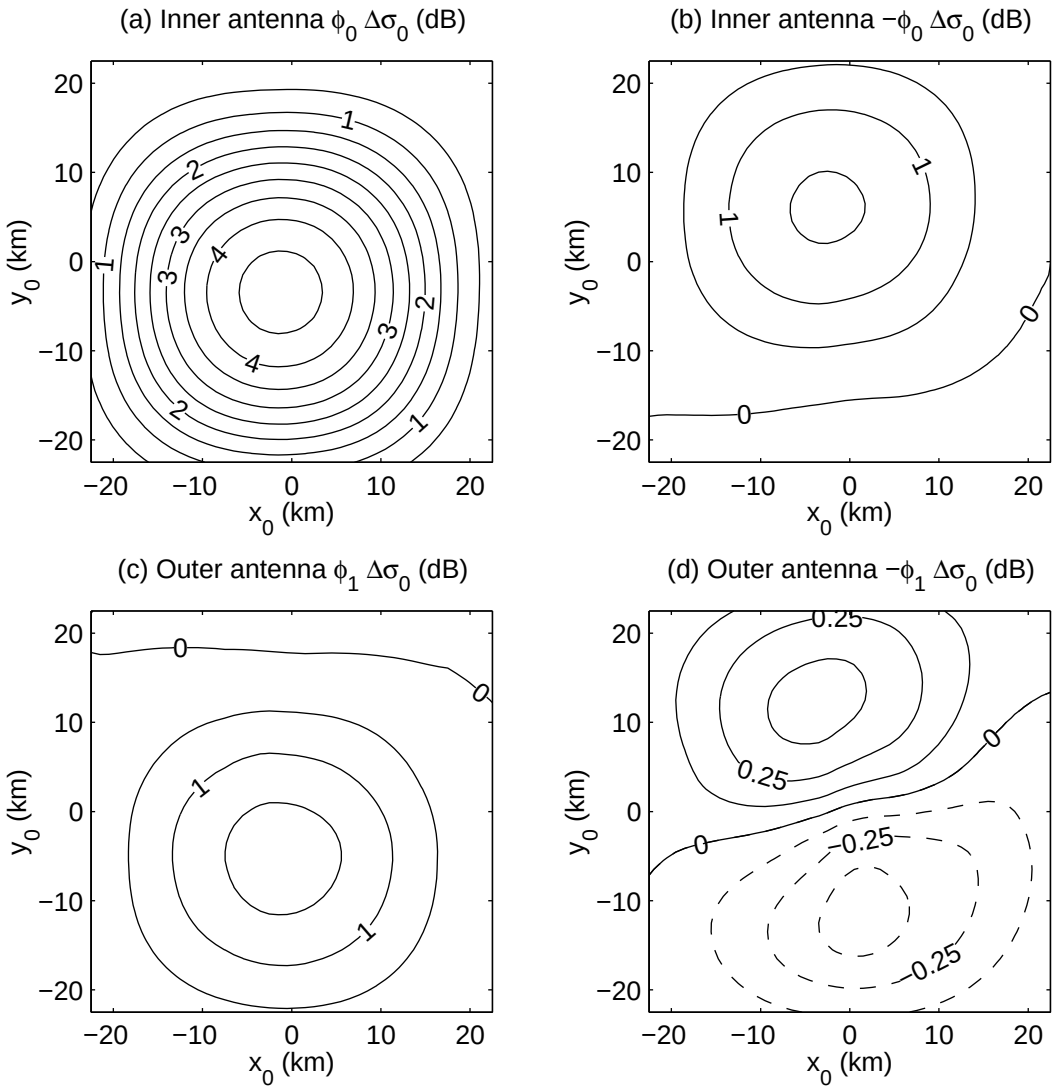
(a) Inner antenna ϕ_0 $\Delta\sigma_0$ (dB)
(b) Inner antenna $-\phi_0$ $\Delta\sigma_0$ (dB)
(c) Outer antenna ϕ_1 $\Delta\sigma_0$ (dB)
(d) Outer antenna $-\phi_1$ $\Delta\sigma_0$ (dB)
x_0 (km)
y_0 (km)
20
10
0
−10
−20
0.25

Fig. 8

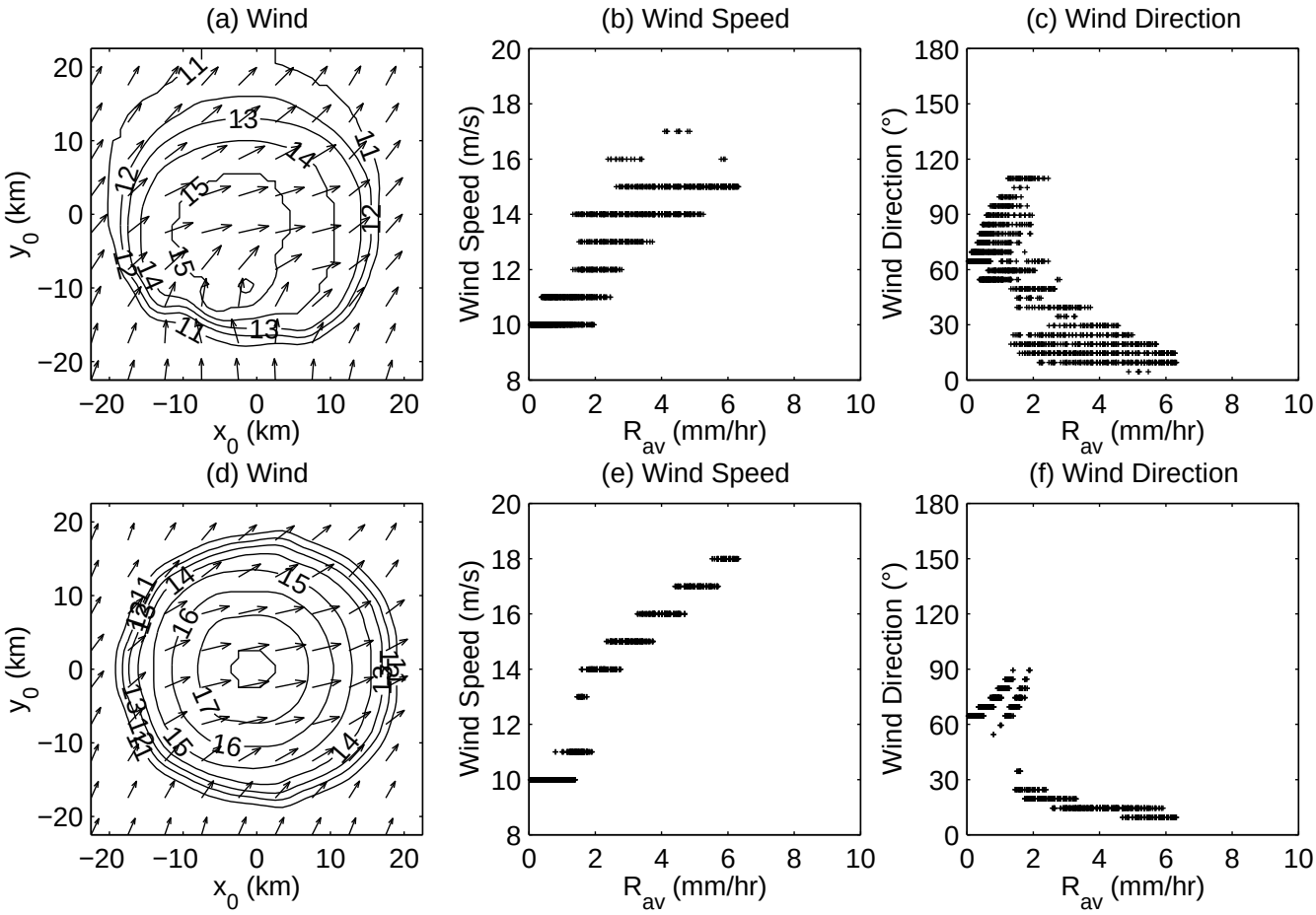
(a) Wind
(b) Wind Speed
(c) Wind Direction
(d) Wind
(e) Wind Speed
(f) Wind Direction
y0 (km)
x0 (km)
Wind Speed (m/s)
Wind Direction (°)
Rav (mm/hr)

Fig 9

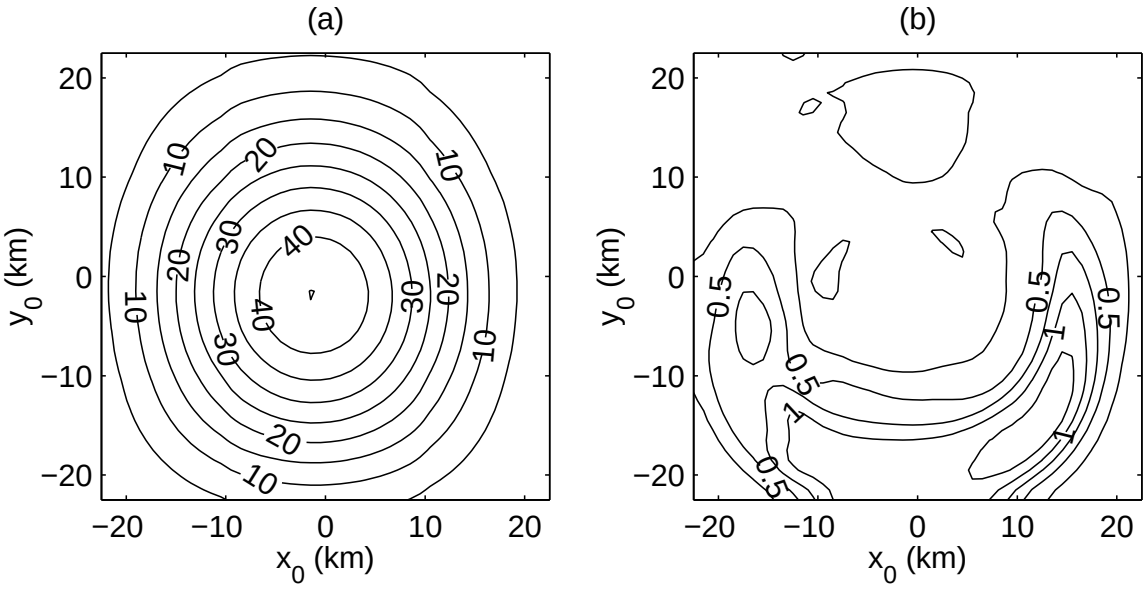

Fig. 10

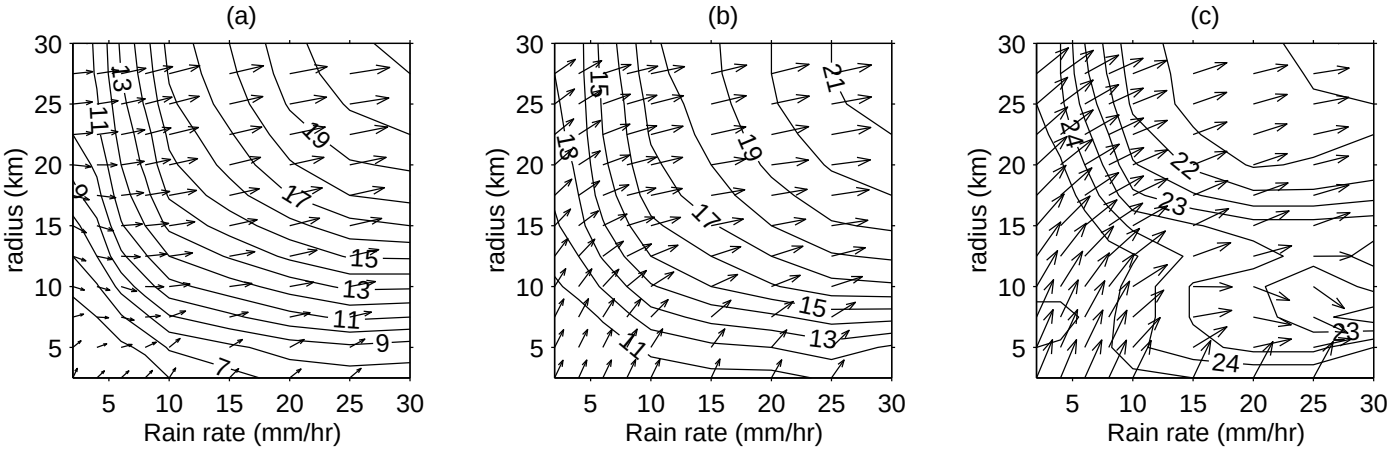
(a)
(b)
(c)
radius (km)
Rain rate (mm/hr)
30
25
20
15
10
5
5
10
15
20
25
30
7
9
11
13
15
17
19
21
22
23
24

Fig 11

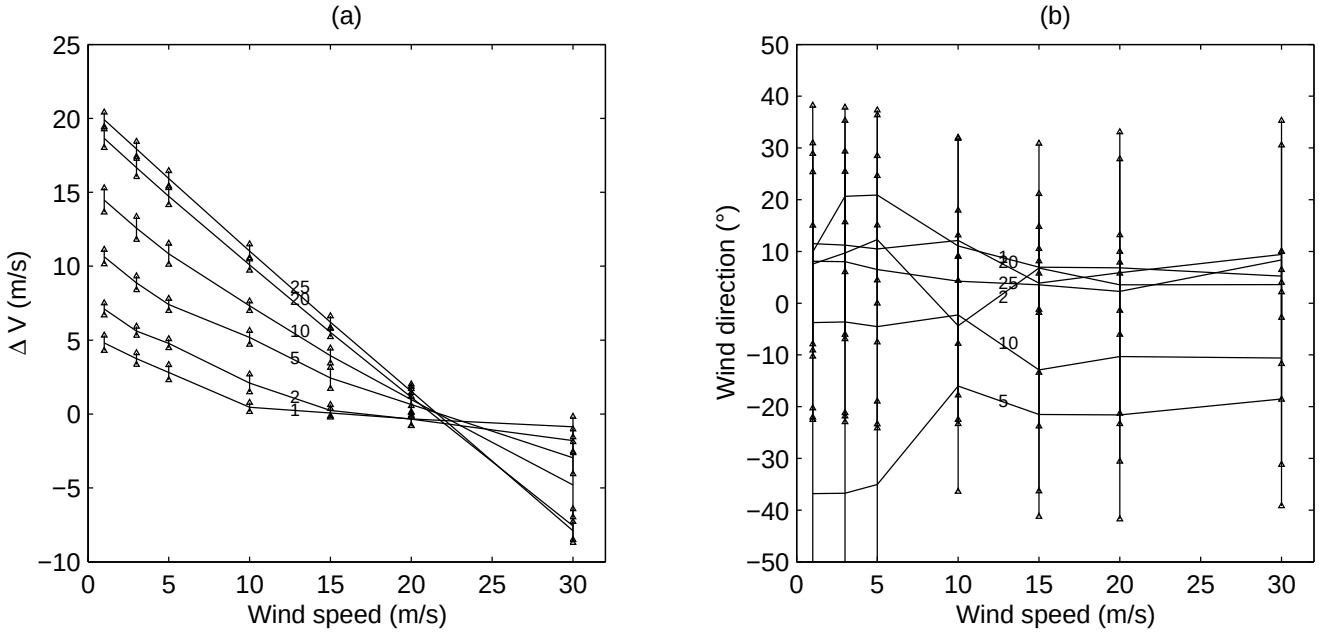
(a)
Δ V (m/s)
Wind speed (m/s)
25
20
10
5
2
1
(b)
Wind direction (°)
Wind speed (m/s)
1
20
25
2
10
5

Fig. 12

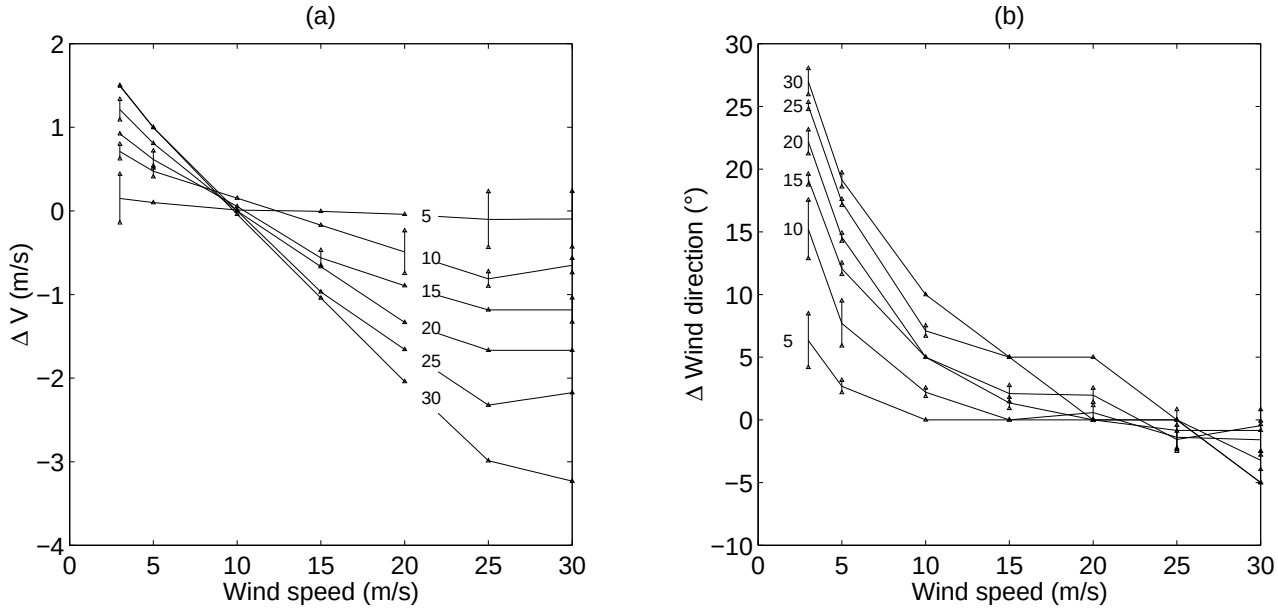
(a)
Δ V (m/s)
Wind speed (m/s)
5
10
15
20
25
30
(b)
Δ Wind direction (°)
Wind speed (m/s)
30
25
20
15
10
5

Fig. 13